Low ice adhesion on soft surfaces: elasticity or lubrication effects?

Catalina Ospina[a], Pablo F. Ibáñez-Ibáñez[a,b], Irene Tagliaro[a], Luca Stendardo[a], Samuele Tosatti[c], Carlo Antonini[a]

Corresponding author: Carlo Antonini carlo.antonini@unimib.it

[a] Department of Materials Science, University of Milano-Bicocca, Via R. Cozzi 55, 20125 Milan, Italy

[b] Department of Applied Physics, University of Granada, Av. de Fuente Nueva, s/n, 18071 Granada, Spain

[c] SuSoS AG, Lagerstrasse 14, 8600 Dübendorf, Switzerland

* Corresponding authors: Irene Tagliaro irene.tagliaro@unimib.it, Carlo Antonini carlo.antonini@unimib.it

Abstract

Hypothesis

Soft materials are promising candidates for designing passive de-icing systems. It is unclear whether low adhesion on soft surfaces is due to elasticity or lubrication, and how these properties affect the ice detachment mechanism. This study presents a systematic analysis of ice adhesion on soft materials with different lubricant content to better understand the underpinning interaction.

Experiments

The wetting and mechanical properties of soft polydimethylsiloxane with different lubricant content were thoroughly characterized by contact angle, AFM indentation, and rheology measurements. The collected information was used to understand the relationship with the ice adhesion results, obtained by using different ice block sizes.

Findings

Three different de-icing mechanisms were identified: (i) single detachment occurs when small ice blocks are considered, and the ice completely detaches in a single event. In the case of larger ice blocks, the reattachment of the ice block is promoted by either: (ii) stick-slip or, (iii) interfacial slippage, depending on the lubricant content.

It was confirmed that the ice adhesion strength not only depends on material properties but also on experimental conditions, such as the ice dimensions. Moreover, differently than on hard surfaces, where wetting primarily determines the icephobic performance, also elasticity and lubrication should be considered on soft surfaces.

Keywords: adaptative wetting, anti-icing surface, hydrophobicity, icephobicity, liquid infused, PDMS

1. Introduction

Designing materials that reduce ice accretion and facilitate its removal from solid surfaces is relevant for many systems operating at low temperatures, in fields spanning from aerospace [1] to marine and ground infrastructures [2], and to domestic appliances [3,4]. This challenge has driven great interest in icephobic materials, a general term used to define systems with surface properties that help to counteract ice accretion, either by preventing ice formation or by reducing ice adhesion.

Based on repellency to liquid water, hydrophobic and textured superhydrophobic surfaces have been widely investigated in the last decade for their potential icephobicity [5–9]. As an alternative strategy, materials with lubricant trapped in the interstices of a rough or porous surface, such as the well-known Slippery Liquid Infused Surfaces (SLIPS) or Liquid-Infused Surfaces (LIS) [10–13], can facilitate the ice release because of the low adhesion between ice and the lubricant layer [14]. However, the durability of SLIPS/LIS surfaces can be compromised due to lubricant depletion after several de-icing cycles.

More recently, a third alternative has emerged: soft polymeric surfaces [15–19]. Soft polymers are interesting because both elasticity and lubrication can be tuned by regulating the ratio among crosslinked and un-crosslinked chains [20]. Soft polymers can be classified as intrinsically lubricated materials due to the presence of mobile chains with dangling ends embedded in the bulk, which provide interesting features like the time-dependency of its contact angle promoted by the presence of humidity [21,22] and the combination of elastic and viscous response, verified in wetting processes where the coupling between elastic and capillary effects has been reported [23,24]. The uncrosslinked molecules dispersed in the bulk material help regenerate the lubricant after repeated icing tests, improving its robustness.

Polydimethylsiloxane (PDMS) is a polymeric rubber that is commonly included in icephobic formulations due to its intrinsic hydrophobicity and modulable mechanical properties [25–30]. Recent studies have shown that tuning the mechanical properties of a PDMS formulation by adding different amounts of unreactive siloxane chains, lowers ice adhesion strength values [28,29]. The delay in solidification of supercooled droplets was also reported in airfoil wing model experiments under dynamic glaze icing conditions [26], in which droplet rebound plays a significant role. Conversely, including a PDMS fraction in a

polyurethane matrix [30], reduces the ice adhesion strength from 70 to 99% compared to the PDMS-free material, even reaching the ice self-shedding by its weight for ice blocks with 1 cm^2 of area in contact with the substrate; in the study, the effectiveness of the designed materials is attributed to the low surface tension components at the ice-substrate interface.

The above reports all show that icephobicity can be achieved by a complex interplay of wettability, elasticity, and lubrication, and it is not trivial to attribute the contribution of the different surface properties to the ice adhesion results of soft polymers.

The long-established state of the art on icephobic materials is based on the premise that the work of adhesion depends on liquid water-substrate interaction and considers the average ice adhesion strength, $\boldsymbol{\tau}_{ice} = F/A$, calculated as the ratio between the adhesion force, F, and the contact area, A. One of the pioneering studies in the field of icephobicity [31] proposed an empirical correlation between the icephobic performance and the wetting properties of smooth, non-deformable materials:

$$\tau_{ice} \propto (1 + cos\,\theta_R) \qquad (1)$$

Where, τ_{ice} is the average ice adhesion strength, and θ_R, is the receding contact angle measured for liquid water. Following that approach, the decreasing of the surface energy will lead to better icephobic performance. In the original and some subsequent papers, Equation (1) was found useful to predict ice adhesion on different smooth elastic materials [31,32], but the equation does not necessarily hold on complex surfaces, such as superhydrophobic or liquid-infused surfaces.

In addition to the wetting, mechanical properties also affect ice adhesion. When a block of ice (Young's modulus E ≈1-10 GPa) is separated from a soft material (typically E < 10 MPa, according to [25]), microfractures are induced at the interface, promoting the easier detachment of ice blocks [33].

The relation among the mechanical properties of a material and its adhesion to a solid, has been adapted from the theory proposed by Kendall [34], originally derived considering a tensile experiment. Based on that work, the force necessary to detach a solid of contact area A from thick glue films is given by:

$$F \propto A\sqrt{\frac{W_{adh}\,K}{\boldsymbol{t}}} \qquad (2)$$

Where W_{adh} is the interfacial surface energy, *t* is the layer thickness ranging from 0.4 to 4.8 mm and K is the bulk modulus of the adhesive material, which, in the mentioned work resulted to be 10 times the Young's modulus E. Equation (2) has been used in several papers to compare the ice adhesion strength of different materials below 500 um thickness in shear tests, using Young or shear modulus [16,28,35,36], despite the initial relation was proposed for tensile tests and considering the bulk modulus, K. The general outcome of those experiments is that the low elastic modulus does not guarantee low ice adhesion performance, but different surfaces with low ice adhesion strength have in common a low elastic modulus [31,32].

At this point, is important to highlight that a material shows different strain responses under different kinds of stress. Young's modulus, *E*, describes the strain response to tensile stress, the shear modulus, *G*, to shear stress, and the bulk modulus, *K*, to compressive stress. The theoretical relation among them is approximated in the literature for isotropic and homogeneous materials as, $\mathrm{E} = 2\mathrm{G}(1 + \mu)$, where μ is the Poisson's ratio. For PDMS, μ value is generally taken as 0.5 [37], giving a ratio of 3 between the *E* and *G* modulus, indicating that the material will present higher resistance to be stretched or compressed than to be sheared. This fact can give light to the different performances that a material can exhibit in shear and tensile ice adhesion tests [28]. The reported mechanical properties for PDMS give *E* values obtained by Dynamical Mechanical Analysis [16,38], AFM indentation [39], tensile [40,41], and compressive tests [28], in the range of thousands of kPa, with small variations that may depend on the specific curing procedure. On the other hand, shear modulus, *G** measured by previous studies [26,35,41–43], shows values in the range of some hundreds of kPa, which shows that the above relationship between *E*, *G,* and *K* does not hold, indicating that for PDMS does not behave as an ideal rubber, has it has been previously highlighted [44].

Based on the above-discussed framework, the empirical relations that are useful to predict the icephobic performance based on the wetting or mechanical properties are not trivial to apply in the case of soft polymeric solids, suggesting the need to answer a fundamental question: What is more relevant for reducing the ice adhesion, the elasticity of the substrate or lubrication effects, given by the presence of a mobile fraction?

In addition to the complexity of viscoelastic materials, the lack of standard methods for ice testing brings out reported ice adhesion strength values for PDMS with similar compositions ranging from 100 to 5 kPa.

The strong dependence of the results on the experimental methods, where the ice adhesion strength shows significant non-systematic variations on the same material using different ice detachment tests [45,46], and different testing conditions like the ice nucleation temperature, shear and tensile contribution of the applied effort and its velocity, and the size of the ice block considered [16], together with the poor description of the detaching mechanisms make the comparison of different materials extremely challenging.

The above-mentioned aspects are fundamental to the discussion about the accurate way to characterize the material properties relevant to the ice adhesion results for a particular experiment. More notably, when the inclusion of a lubricant fraction affects the wetting and the mechanical properties of the polymers at the same time [20,47,48]. In this study, we aim to elucidate the contribution of elasticity and lubrication in ensuring the icephobicity of soft polymeric materials. By systematically controlling the content of movable chains, i.e. lubricant, in a PDMS formulation (Figure 1), both wetting and mechanical performance were assessed. Different ice detachment regimes were identified and their relationship with material properties is discussed to understand the effect of the individual parameters on ice detachment mechanisms.

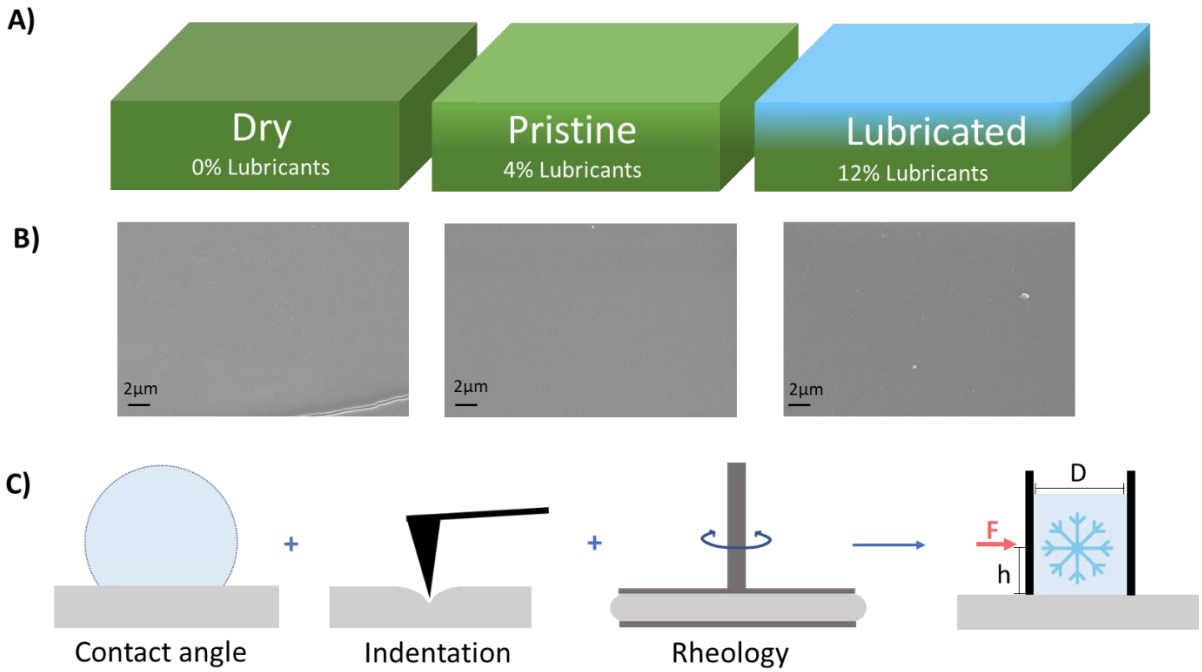

Figure 1. a) Representation of the PDMS (10:1 base to crosslinker ratio)-based samples with different lubricant content. The samples are named referring to the lubricant content. The dry sample represented in dark green has been extracted to obtain 0% lubricant; the pristine sample represented in light green contains 4% lubricants from the base formulation; the lubricated sample represented in blue is loaded with additional lubricant to reach 12%). b) SEM microscopy of the samples obtained at 10KX magnification. c) Schematic of contact angle, indentation, and rheology measurements performed to correlate material properties with icephobic performances, where the pushing height is h=1mm and the ice block diameter D is varied from 8 to 14mm.

2. Materials and methods

2.1. Soft surface fabrication

The samples in Figure 1 were obtained using Sylgard 184 (Dow Corning), which is a two-component silicon elastomer consisting of base and crosslinking fractions. The main formulation is obtained by mixing the base and crosslinker in 10:1 proportion. Pristine samples were fabricated by depositing in a glass slide (2.5 × 7.5 cm^2) the appropriate amount of main formulation to reach 1.1± 0.2 mm thickness material, followed by a curing process for 2h at 80°C. Dry samples were obtained with the same procedure, followed by soaking the as-prepared pristine samples in toluene for 48h, changing the solvent every 24h, which extracts the uncrosslinked chains (≈4% by weight) in the polymer [21]. Lubricated samples differ from dry and pristine only by the addition of 8% silicone oil (viscosity of 20 cSt, Sigma Aldrich) to the main formulation, added before the crosslinking treatment at 80°C, leading a total content of 12% lubricant in the sample.

2.2. Contact angle measurements

Sessile drop experiments were performed on the different samples, using a custom-built setup composed of a High-speed Camera (PHOTRON NOVA FASTCAM S6, Venus Laowa 100mm *f*/2.8 2× Ultra Macro APO lens, JJC Auto Focus Extension Tube 20 mmm) and a Liquid inlet (Pump 11 Pico Plus Elite from Harvard Apparatus).

The procedure is the following: (i) deposition of an initial 3 µL droplet, (ii) 3 s pause for drop stabilization and oscillation dampening, (iii) drop inflation at a constant rate of 3 µL/min to reach a maximum drop volume of 8 µL, (iv) drop deflation at a constant rate of 3 µL/min. The video of the experiments was recorded at 10 fps. The advancing and receding contact angle were calculated in the Dropen software [49], developed in MatLab environment using the circle fitting. The reported data includes a minimum three independent measurements.

2.3. AFM indentation for mechanical properties

The Young's modulus of the samples was assessed by AFM indentation analysis with the Atomic force microscope (Core AFM from Nanosurf). Using the contact mode, a nanometric tip (PPP-CONTR-10 tips with radius = 0.010 µm, Res. Freq= 12kHz and spring constant= 0.12 N/m) is approached and retracted to the sample while its deflection is registered. The indentation depth was 1 µm and the sensitivity was calculated by using a glass slide as a hard material reference, which is used to convert the voltage to the actual displacement in the cantilever. In the penetration region, the Johnson-Kendall-Roberts model is used to fit the curve slope and obtain the material Young's modulus, E. All the experiments were performed avoiding high humidity conditions. The reported results are averaged from ten independent experiments.

2.4. Rheology test

The sample shear (G') and loss (G'') moduli were evaluated in an MCR92 RheoCompass™ rheometer from Anton Paar. By approaching the parallel plates of 25 mm diameter, using the viscoelastic moving profile, the samples of ~0,9mm were compressed until the safe gap was reached, by compressing the sample less than 12% of its thickness. A preliminary amplitude sweep was first conducted, selecting a strain amplitude of 1,5% to perform the frequency sweep between 1 and 100 rad/s. Reported results are taken at 100 rad/s and are the average of five independent measurements.

2.5. Ice adhesion measurements

To verify if differences in surface wetting affect the ice adhesion on a soft surface and elucidate the role of elasticity and lubrication, horizontal ice adhesion push tests (i.e. shear detachment due to a lateral force) were conducted on the three PDMS samples with different lubricant contents, changing the ice block diameter, D. The tests were performed in a custom-built setup consisting of a horizontal shear test, which has been fully described previously [50,51]. Briefly, the setup includes an environmental chamber, different from real to application conditions, and to obtain clear ice that allows visualizing the fracture propagation by controlling the location of the ice nucleation freezing front, a Peltier element was used to cool the substrate, and a motion stage connected to a force transducer to apply a load on the ice block. The ice was formed by using cylindrical nylon molds of 8 to 14mm inner diameter to form the ice. Since impurities could uncontrollably affect the measurements, distilled water was used. The liquid water was deposited at 0° C and then, the surface of the sample was cooled down to reach -10°C. After freezing, the ice was allowed to stabilize for 20 min while the relative humidity was maintained close to ~3% by low nitrogen flow. A force probe was then pushed against the mold containing the ice at a 1 mm distance from the substrate with a constant velocity so the applied force on the ice increased until ice detachment events occurred. A preliminary screening of pushing velocity has been done for the pristine material and is available in the Supplementary information (S1). The selected velocity is then 10 μm/s, to simulate a quasi-static response and avoid the velocity effects. The experiment was video recorded from the top of the ice cylinder through the clear ice using a phone camera with a resolution of 1920x1080 at 30fps to correlate the peaks in the force/time plots with the fracture events (Supplementary videos S1, S2, and S3).

3. Results and discussion

To provide a complete material characterization, the wetting and mechanical properties of PDMS with different lubricant content were analyzed by contact angle (Figure 2a), AFM indentation (Figure 2b), and rheology (Figure 2c) measurements. A summary of the results

is also presented in Table 1. They will be analyzed in detail in sections 3.1 and 3.2, which are later related to the ice adhesion results in section 3.3.

In the supplementary information the optical images and SEM microscopies of the samples are presented (S2 and S3). The surfaces are visually smooth, with an estimated roughness of 20nm reported previously for materials with similar composition and fabrication methods [52,53].

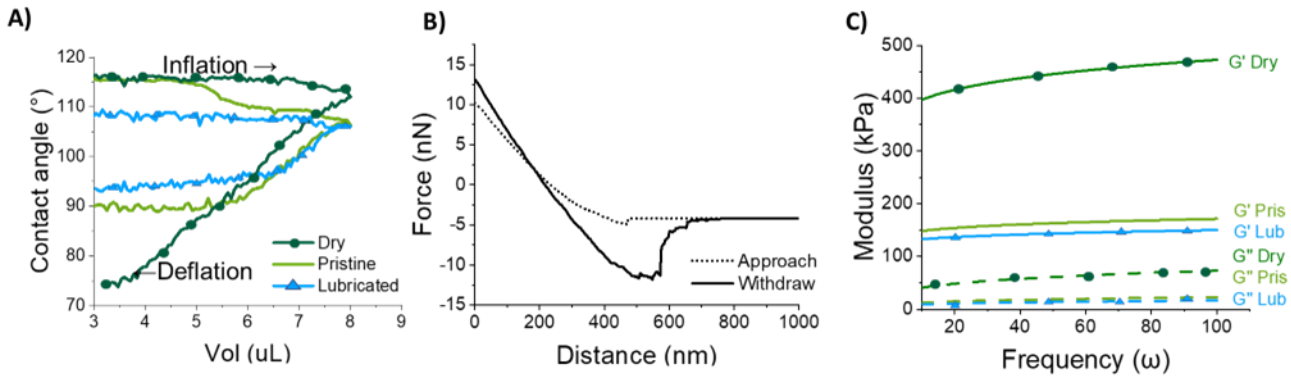

Figure 2. Characterization performed on PDMS samples. Dark green represents the dry, light green the pristine, and, blue the lubricated sample. a) Contact angle in a sessile drop experiment. b) Nanoindentation graphs using an Atomic Force Microscope with a contact mode tip of 10nm radius. Force curves were visually similar for all three samples; the curve for the Pristine sample is shown as reference. c) Rheology experiments in frequency sweep tests: the continuous line represents the storage, and, the dashed line is the loss modulus.

Table 1. Data from sessile drop experiments and mechanical properties (AFM indentation and rheology) for the three samples: dry, pristine, and lubricated PDMS.

	Contact angles			AFM indentation	Rheology	
	θ_A (°)	θ_R (°)	$\Delta\theta$ (°)	E (kPa)	G* (kPa)	tan δ
Dry	117±1	74±2	43±2	3060±660	477±94	0.16±0.002
Pristine	109±3	91±1	18±3	2983±560	171±16	0.13±0.005
Lubricated	107±2	96±1	11±2	2508±620	146±12	0.11±0.002

3.1. Wetting properties

The wetting properties of the PDMS samples were characterized by measuring the advancing θ_A and receding θ_R contact angle using the sessile drop method. In Figure 2a, it is possible to see the evolution of the contact angle during drop inflation and deflation; θ values and the contact angle hysteresis calculated as $\Delta\theta = \theta_A - \theta_R$ are also summarized in Table 1 for convenience. The three samples show different wetting behaviors. The dry sample, plotted in dark green in Figure 2a, presents a constant θ_A=117° during the whole inflation phase, and starts receding in the deflation phase for θ_R=74°, with a relatively high contact angle hysteresis, Δθ = 43°. For the lubricated sample, plotted in blue in Figure 2a, the hysteresis decreases significantly, with θ_A=107°, θ_R=96°, and Δθ = 11°. The pristine sample, plotted in a light green line in Figure 2a, shows an intermediate behavior, denoting a clear transition of wetting properties during the experiment itself. At the beginning of the experiment, the contact angle is θ=117°, which corresponds with that θ_A of the dry sample; however, when the volume reaches 5 µl (see Figure 2a), after ~40 s from the beginning of the experiment, the contact angle decreases to reach a value of θ_A =109°, similar to the θ_A of the lubricated sample. This phenomenon has been previously described as adaptative wetting behavior [21] and has been explained with a migration of lubricant molecules from the bulk to the PDMS-water interface, which leads macroscopically to a modification of the wetting properties. During volume deflation, the contact line is initially pinned and then starts receding at a θ_R =91°, slightly lower than lubricated PDMS. In the summary reported in Table 1, we have deliberately chosen and indicated the value θ_A=109° for the pristine sample, as this is more relevant given the ice adhesion test protocol, where the water and the samples are in contact for a long time (in the order of minutes) before freezing occurs.

The wetting experiments (Figure 2a and Table 1) showed a decrease in contact angle hysteresis values when increasing the lubricant content, a clear indication of the presence of a movable layer at the interface. In previous studies, it has been previously stated that the hydroxyl units at the interface are relevant for the ice adhesive performance whereas the methyl units are important in the de-bonding events [44]. The experiments presented here evidenced that the hydroxyl units at the surface of the PDMS reorganize upon contact with water, exposing the hydrophilic dangling ends to the interface, and affecting its wetting properties, which depend on the previous contact with water.

3.2. Mechanical properties

The mechanical properties of the PDMS samples were assessed by AFM nanoindentation and rheology experiments. Tests were performed without any pre-wetting treatment of the samples to avoid surface reorganization due to the previously verified adaptative wetting behavior.

In Figure 2b, the black line in the indentation experiments indicates that the three different samples showed similar responses, therefore, all three tested PDMS samples have similar Young's Moduli, E, in the range 2.5-3.1 MPa (see Table 1), with no effect of the lubricant content, as differences are not statistically significant (t-test distribution, with 95% confidence).

To assess the mechanical behavior of the material when shear stress is applied, similarly as in the performed ice adhesion tests, the samples were evaluated by oscillatory rheology tests, by measuring the storage, G', and loss, G'' moduli, as a function of the angular frequency, ω.

The results illustrated in Figure 2c, where the dark green graphs represent the dry, light green the pristine, and, blue the lubricated sample, indicate a predominant elastic response for all the samples (G'>G'') in the investigated frequency range. It is possible to further investigate the ability of the material to store and dissipate energy by calculating the complex shear modulus, $G^* = \sqrt{G'^2 + G''^2}$, which considers the combined contribution of elastic and viscous response and the ratio of the viscous to elastic effects, represented as the tangent of the phase angle δ, with tan δ = G''/G'. In Table 1, the G* and tan δ values calculated for ω =100 rad/s are summarized. Due to the inclusion of lubricants, the complex shear modulus decreases strikingly from G*=477±94 kPa for the dry sample, which contains no lubricants, to values of 171±16 and 146±12 kPa for pristine and lubricated PDMS, respectively.

Regarding tan δ, they are all in the range 0.11-0.16, well below 1, confirming that PDMS response is primarily elastic. Notably, G^* is an order of magnitude smaller than E. As discussed in the Introduction section, these values are in line with previous observations for PDMS with similar composition, where E values are in the range of thousands of kPa [16,28,38–41], and G^* is in the range of some hundreds of kPa [26,35,41–43].

The study of the mechanical properties of the PDMS may suggest a possible phase segmentation that affects the isotropic character of the samples. The experimental evidence makes it worth considering the possible segmented structure of the lubricant dispersed in discrete agglomerates within the elastomeric network [15,54] that can store energy and avoid its dissipation in the material bulk.

3.3. Icephobic performance

To provide a synthetic overview of different ice adhesion experiments, a representative time evolution of the push force for each sample and ice block diameter is illustrated in Figure 3a. In all the cases, the force initially increases and the shear stress is accumulated at the interface until reaching a maximum, where a drop in the force is observed. The top-view video recording enables us to observe the simultaneous ice detachment from the substrate and its evolution at the ice-PDMS interface, allowing us to correlate the fracture propagation with the force measurements.

When the maximum peak has been reached, however, different scenarios are observed both in the evolution of the push force in Figure 3a and by the visualization of fracture events (Supplementary videos S1, S2, and S3). Three different ice detachment mechanisms can be identified: (i) single detachment, (ii) stick-slip, and (iii) interfacial slippage, as schematized in Figure 3b.

The single detachment regime occurs with ice blocks of 8 and 10 mm diameter (see Figure 3a, blue box). It is characterized by the existence of only one force peak. As soon as the maximum force F_{max}, (represented as a black arrow in Figure 3a) is reached, the fracture grows at the interface in the direction of the applied effort (see Supplementary. video S1) and the force curve reduces from F_{max} to zero, denoting a complete adhesive failure between ice and PDMS. It is worth noticing that the force peaks present a rounded shape, different from rigid surfaces, where is typically observed a sharp peak detachment and a fracture propagates in the order of milliseconds [50]. In the case of soft materials, the fracture propagation in the supplementary videos S1, S2, and S3 occurs in the range of seconds, so it can be thus visualized with a standard camera. Furthermore, the rounded-shaped peak of the force curves indicates that some of the energy liberated in the initial detachment is absorbed by the material and used for its lateral deformation before the fracture grows [35], slowing down the crack speed, when compared with rigid materials [47,55].

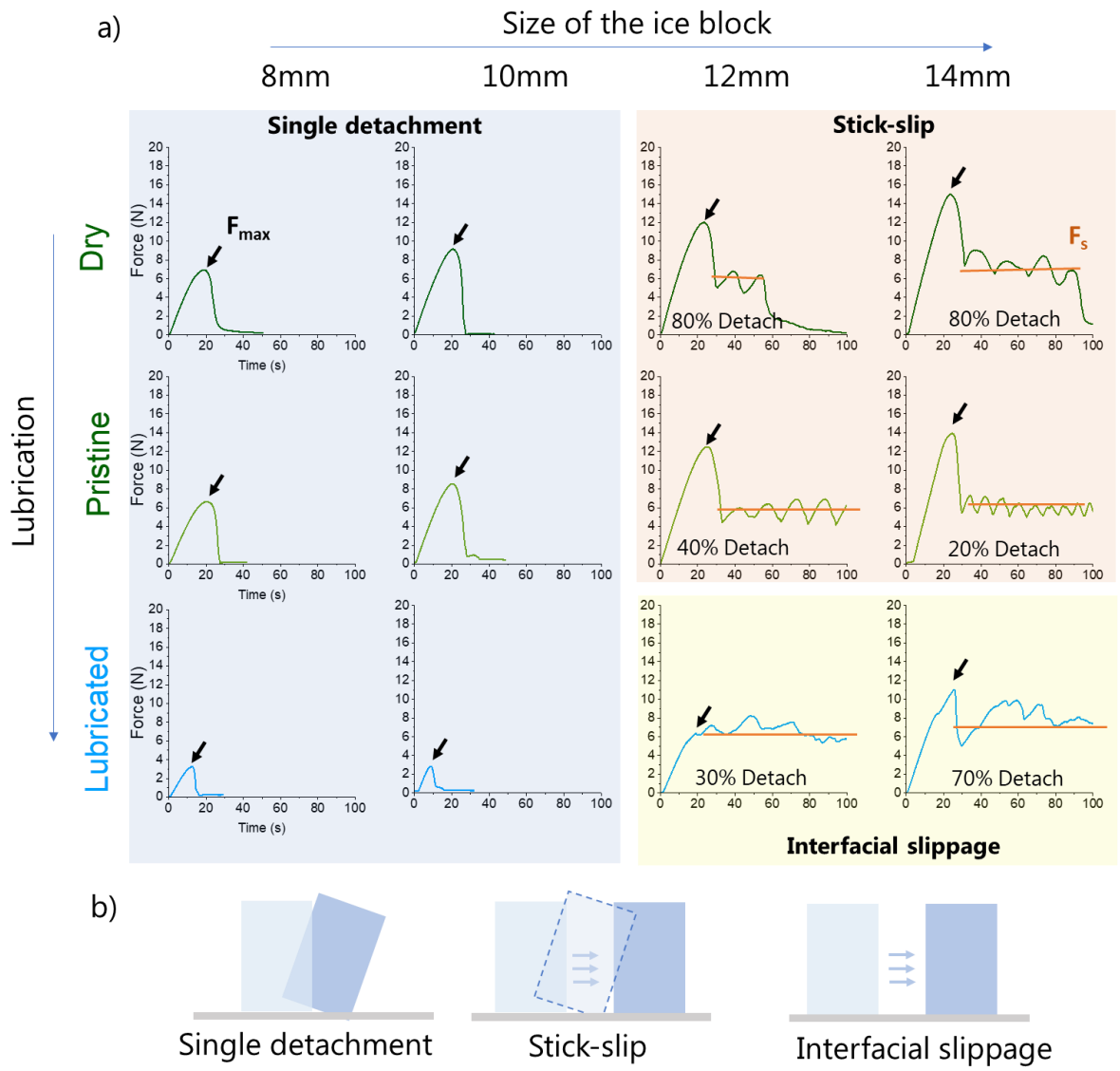

Figure 3. a) Force vs time curves of the ice adhesion tests for PDMS samples with different lubricant content at 1mm pushing height varying the size of the ice block. Each plot is representative of six different measurements. Three different detachment mechanisms are identified in the experiments. At small sizes, the ice detaches in a single event (blue box). When using larger ice blocks, the experiment takes longer because reattachment occurs giving different scenarios: The stick-slip, in the orange box and interfacial slippage, in the yellow box. b) Schematic representation of the three different detachment mechanisms identified in the experiments. Representative videos of the different mechanisms are available in the Supplementary videos S1, S2, and S3.

For larger ice dimensions, when using ice blocks of 12 and 14 mm diameter, two ice detachment phases can be identified: in the first "static" phase, the force reaches a peak (F_{max}); and in the second "dynamic" phase, ice moves along the interface, while still partially

adhered, with the force oscillating around an average value, F_s, represented as an orange line in Figure 3a. The regular way to evaluate the icephobic performance, which relies on the comparison of F_{max}, ignores the fact that after an initial detachment, the ice can reattach and remain adhered. It makes it worth considering not only the first peak but also the secondary peaks, that reveal different mechanism among samples with different lubricant contents.

Figure 4 graphically summarizes the values of F_{max} and F_s averaged values from Figure 3a for the three different samples. Figure 4a, b and c) refer to F_{max}. Figure 4d, e, and f) refer to F_s, where there is no data for 8 and 10mm diameter ice blocks because in those cases the ice presented a single detachment.

The dry and pristine samples show similar stick-slip behavior, also referred to in the literature as separation pulse [56], with a high initial peak force, F_{max}, followed by force oscillations in the dynamic phase around F_s. Nevertheless, the presence of uncrosslinked chains in the pristine PDMS promotes continuous sliding compared to the dry PDMS, where the force eventually decreases to zero (Figure 4a). The stick-slip dynamic regime is characterized by the regular pattern of fracture propagation in which the force oscillates around F_s (see Figure 3a, orange box). In the Supplementary Video S2, it is possible to identify the interfacial separation that propagates from front to back (corresponding to left-to-right in the video) i.e. in the direction of the applied force F. When the maximum deformation of the coating is reached, the ice separates from the substrate and, due to the elastic recovery of the material and the silanol dangling ends at the interface, it re-attaches while moving from its original position, generating a cyclic fracture propagation [57], identified in the bibliography as a separation pulse [58]. When the attachment-detachment or stick-slip cycles [35], present a regular pattern, the adhesion energy and the ability to store elastic energy are comparable, and the velocity of the crack opening edge and the velocity of the crack closing edge are equal to each other[59].

The lubricated PDMS shows instead interfacial slippage: after reaching the first peak, the force oscillates around this value, i.e. $F_{max} \approx F_S$. In Supplementary Video S3, the separation pulses generated at the interface overlap with irregular slip pulses, in which the material slides without a clear interface separation pattern [60]. The mechanical instabilities promote the release of shear energy, where a part of the substrate is detached from the ice but sticks again after some time. This creates a non-contact region at the interface that is propagated

in the direction of the applied force, giving a non-regular pattern in the force curves (see Figure 3a, yellow box and Supplemetary Video S3).

For dry and pristine samples, the crosslinking density is maintained constant, whereas for the lubricated sample, the non-reactive chains of the silicone oil, added before the thermal curing, may decrease the crosslinking density [61]. By increasing the lubricant content and decreasing the crosslinking density, the interfacial slippage is enabled in the lubricated sample, and ice can slide over the sample without proper detachment from the load-bearing chains [20], because they present relative motion compared to the static bulk solid.

From the results in Figure 4, it is possible to note that the size of the ice block is relevant in the detachment mechanism: with a smaller ice dimension, the single detachment regime is observed for soft materials irrespective of the lubricant content. By increasing the ice dimensions, the reattachment can be promoted, giving different mechanisms depending on the lubricant content (Figure 3b).

The most common approach to compare the icephobic performance of two different substrates is to report the first detachment peak F_{max}. In Figure 4a it is evident how the lubricant content plays an important role in decreasing ice adhesion. Therefore, the lubrication effect in icephobic performance cannot be neglected. Nevertheless, this decrease cannot be explained by considering only the wetting properties with Equation (1) since the pristine and lubricated samples present similar θ_R, however, the ice adhesion results show different behavior. Consequently, the wetting properties, represented by the receding contact angle, are not sufficient to predict the ice adhesion strength of soft materials with different lubrication degree [20]. On the contrary, the lubricated sample, with lower shear modulus and likely lower crosslinking density has the lowest ice adhesion values, irrespective of the dimension of the ice block.

The F_{max} trend in Figure 4a indicates an effect of the size of the ice block. One common approach to considering the size effects is to divide by the total area in contact and report $\tau_{ice} = F/A$, where A is the contact area. Data in Figure 4b suggest that τ_{ice} is approximately constant only on the lubricated PDMS. On dry and pristine PDMS, the maximum force F_{max} does not scale with the area ($A \propto D^2$). This has important consequences, as it means that τ_{ice} is not an intrinsic material property, since it depends on the experimental conditions, i.e.

412 the ice block size in our test. In Figure 4c, aiming to identify the change in the mechanical
413 fracture mechanism where the force becomes independent of the ice dimensions[62], we
414 reported the F/D trend, which is also not constant, as it increases slightly with D. Indeed,
415 data fitting with the power law $F \propto D^{\alpha}$, for dry and pristine PDMS gives values of α in the
416 range 1.3-1.6, but a more accurate estimate would require testing of ice blocks with larger
417 diameters, which are beyond the size that can be tested on our setup.

418 In this regard, based on classical fracture theory for rigid materials, it has been recently
419 highlighted that the average ice adhesion strength, τ_{ice}, has to be measured in the correct
420 conditions since strength controls detachment for small ice block sizes (with dimension $L<L_c$,
421 a critical length) and toughness controls detachment for large ice block sizes ($L>L_c$). For
422 hard surfaces, interfacial toughness Γ can be estimated assuming only the elasticity of ice,
423 as $\Gamma \approx \tau^2 L_c^2/2E_{ice}h$, where τ is the adhesion strength, E_{ice} the ice, h the ice block thickness,
424 and L_c is measured from experiments [50,62]. As observed in [62], where rectangular ice
425 blocks with fixed width were used, in a toughness-dominated regime, above a critical length
426 scale, the force becomes independent from the ice block length: this is because the force is
427 needed to trigger an initial crack, that then propagates over the full ice block length.

428 For soft polymers, the use of the above equation for interfacial toughness is questionable,
429 as it does not account for substrate elasticity. Moreover, in our set of experimental data, we
430 see no transition from one regime to the other in the ice block dimension considered,
431 indicating that the toughness-mediated fracture is not reached since the energy released in
432 the fracture cannot extend over the whole ice length. Instead, this energy is absorbed by the
433 coating and used for its deformation [63]. Therefore, the classical mechanical fracture
434 models for hard materials cannot be directly applied to systems that include a soft,
435 deformable non-elastic material.

436 This issue helps to explain the strong scattering reported in the literature in terms of
437 average ice adhesion strength, τ_{ice}, for the same material, in addition to the different ice
438 accretion conditions [16].

439 On the other hand, in the dynamic regime, for bigger ice blocks (Figure 4d,e, and f), it can
440 be noticed that F_s values are very similar irrespective of the dimensions of the ice blocks or
441 the loaded lubricant content. Due to the uniformity of the component nature in the different
442 materials, the dynamic regime would depend more on the viscosity of the lubricant and its

internal friction in the crosslinked network. The results suggest that in conditions where the dynamic phase occurs, it is not possible to further reduce F_{max} below F_s, since it is the characteristic frictional force in the elastomeric network [20,40,61]

Finally, this study confirms the strong dependence of ice adhesion results on experimental conditions. It is worth to mention that, aiming to overcome that issue, in the last year few studies introduced and provided the parameter ARF (adhesive reduction factor), computed as the ratio between the ice adhesion force for reference material, e.g. aluminum, and the one for the material of interest [64–66]. The ARF enables a direct and fair comparison and implicitly recognizes that the average ice adhesion strength, τ_{ice}, depends not only on the material properties but also on experimental methods and test parameters. Consequently, the ice adhesion comparison only makes sense when testing ice adhesion on different materials in the same conditions. The clear limitation is the ARF is dependent on the specific testing and could thus be acceptable only for coating preliminary assessment: tests in close-to-application conditions, e.g. in an icing wind tunnel, are definitely required for a comprehensive icephobic coating assessment.

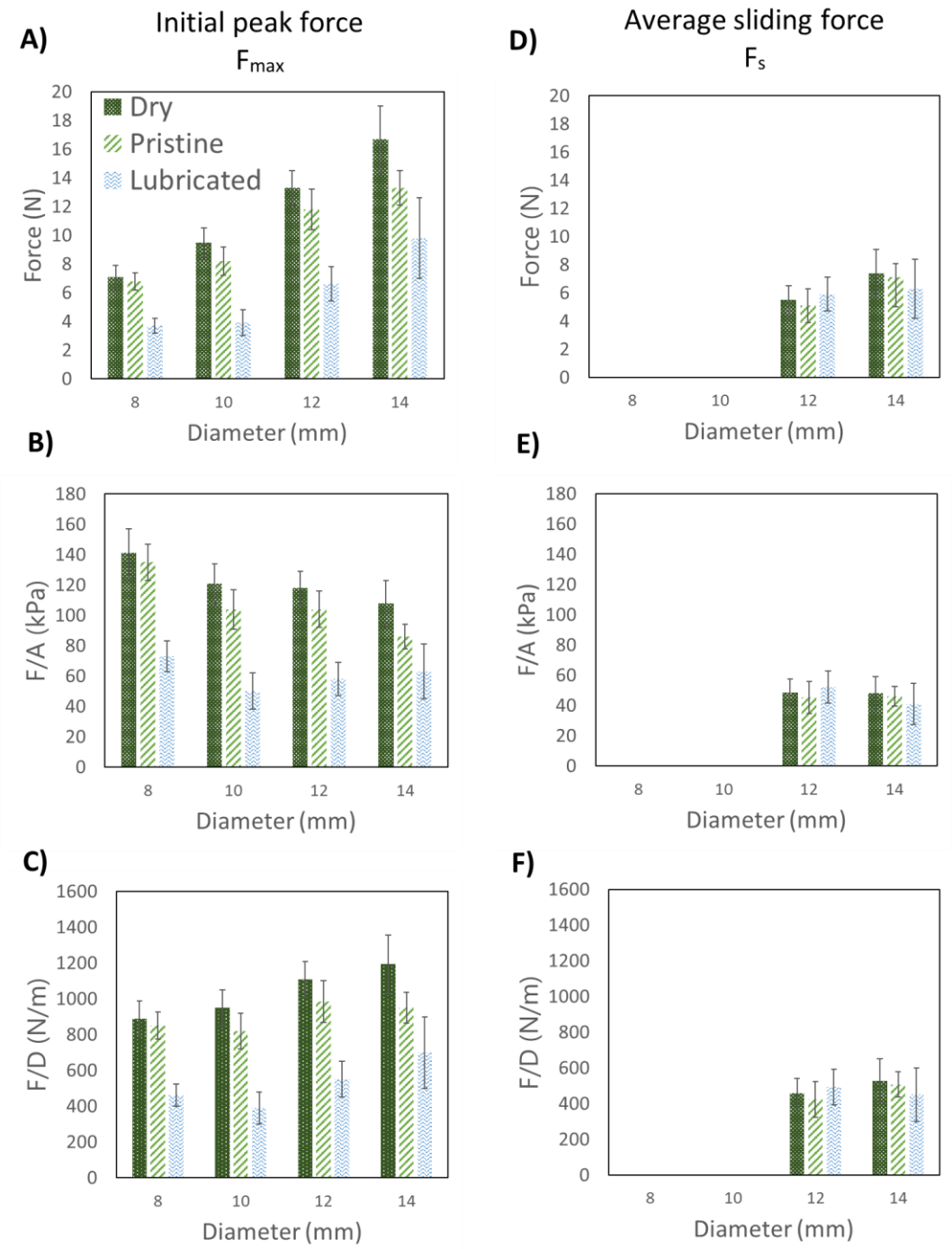

458

459 *Figure 4. Results of ice adhesion tests for samples with different lubrication degrees and different ice dimensions.*
460 *Dark green corresponds to dry, light green to pristine, and blue to lubricated PDMS samples. a) Average measured force*
461 *for initial detachment F_{max}. b) Ice adhesion strength $\boldsymbol{\tau}_{ice}$ (F/A) for initial detachment. c) F/D for initial detachment. d)*
462 *Average force for sliding, F_s. e) Ice adhesion strength for sliding (F_s/A). f) Sliding force divided by the diameter (F_s/D).*

4. Conclusions

Due to the recent interest in soft materials with icephobic properties, the aim of this study was to understand the underpinning mechanism leading to low ice adhesion on soft substrates, focusing on the contribution of lubrication.

The time-dependency of the contact angle, previously reported in soft polymers [21,22] was confirmed and, for the first time, its effect on the ice adhesion properties was verified. Our study confirms that the wetting properties, primarily represented by the receding contact angle [31] in the context of ice adhesion tests for rigid surfaces, are not able to explain and predict the icephobic behavior of soft polymer, as previously shown [20]. This implies that the models that explain the icephobic behavior based on the work of adhesion on liquid water-substrate interaction need to be reconsidered in the case of soft polymers, to also include the relevance of adaptative wetting [21].

By studying the mechanical properties of the PDMS, a widely used soft polymer, we identify the material as a viscoelastic non-ideal rubber, as it has been verified by previous authors using different methodologies [44]; such properties need to be considered when investigating material icephobicity.

Specifically, in the de-icing experiments performed in this study, three different ice detachment mechanisms were identified and characterized on soft surfaces: (i) single detachment, (ii) stick-slip, and (iii) interfacial slippage. The parameters controlling the detachment mechanisms are both the degree of lubrication and the ice block size and a corresponding map has been identified. It was found that the higher lubricant content in soft materials promotes a decrease in the shear modulus and, similar to previous studies [28–30], a decrease in the force necessary for the initial ice detachment, which is an advantage in a single detachment regime, where the small ice blocks are completely separated at the end of the experiments.

When bigger ice blocks are tested, the reattachment of the ice block is promoted, leading to a stick-slip regime for dry and pristine PDMS; differently, an interfacial slippage regime is observed for lubricated PDMS. As such, lubrication content due to uncrosslinked chains needs to be assessed and reported when fabricating and testing the icephobic performance of new soft materials, together with traditional wetting and mechanical characterization.

493 The results and techniques discussed in this work apply to systems composed of
494 elastomeric polymer networks infused with liquid short-chain lubricants. Therefore, other soft
495 non-polymeric materials like carbon soot may present a de-icing mechanism similar to the
496 elastic non-deformable material.

497 It is essential to remark that τ_{ice} is not an absolute value, since it relies on experimental
498 conditions: as such, it cannot be considered an intrinsic material property and can only be
499 used for a relative comparison among materials tested in the same conditions. Moreover,
500 the report of the solely maximum value in the force-vs-time curves, does not describe the
501 diverse mechanisms that can be involved in the de-icing process; therefore, the ice
502 detachment regime has to be reported, together with F and τ_{ice} values.

503 As a future perspective, it will be interesting to assess the potential of the so-called
504 slippery covalently-attached liquid surfaces (SCALS), characterized by nanoscale thickness
505 and anti-adhesive properties, as they have shown similar properties to lubricant-infused
506 surfaces, with hybrid solid-liquid behavior, and thus may be suitable in the context of icing
507 [67,68]. In addition, understanding the adhesion of a solid on a soft surface can be further
508 extended to other fields of application, e.g. vat polymerization in additive manufacturing: at
509 the vat base, where light is irradiated to induce photopolymerization, lubricated soft materials
510 are used to reduce the interfacial adhesion between polymerized resin and the vat base.[69–
511 71]”

References

1. Huang, X.; Tepylo, N.; Pommier-Budinger, V.; Budinger, M.; Bonaccurso, E.; Villedieu, P.; Bennani, L. A Survey of Icephobic Coatings and Their Potential Use in a Hybrid Coating/Active Ice Protection System for Aerospace Applications. *Progress in Aerospace Sciences* 2019, *105*, 74–97.

2. Heydarian, S.; Momen, G.; Jafari, R. Icephobicity and Electrical Assessment of Slippery Coating Impregnated with a Stabilized Hydroxyl-Terminated Lubricant for High Voltage Insulation Application. *J Mater Sci* **2023**, *58*, 9264–9281, doi:10.1007/s10853-023-08600-6.

3. Tagliaro, I.; Cerpelloni, A.; Nikiforidis, V.M.; Pillai, R.; Antonini, C. On the Development of Icephobic Surfaces: Bridging Experiments and Simulations. In *The Surface Wettability Effect on Phase Change*; 2022; pp. 235–272 ISBN 9783030829926.

4. Irajizad, P.; Nazifi, S.; Ghasemi, H. Icephobic Surfaces: Definition and Figures of Merit. *Adv Colloid Interface Sci* 2019, *269*, 203–218.

5. Boinovich, L.B.; Emelyanenko, A.M. Anti-Icing Potential of Superhydrophobic Coatings. *Mendeleev Communications* **2013**, 3–10, doi:10.1016/j.mencom.2013.01.002.

6. Li, X.; Zhang, K.; Zhao, Y.; Zhu, K.; Yuan, X. Enhancement of Icephobic Properties Based on UV-Curable Fluorosilicone Copolymer Films. *RSC Adv* **2015**, *5*, 90578–90587, doi:10.1039/c5ra15920b.

7. Yu, D.; Zhao, Y.; Li, H.; Qi, H.; Li, B.; Yuan, X. Preparation and Evaluation of Hydrophobic Surfaces of Polyacrylate- Polydimethylsiloxane Copolymers for Anti-Icing. *Prog Org Coat* **2013**, *76*, 1435–1444, doi:10.1016/j.porgcoat.2013.05.036.

8. Farhadi, S.; Farzaneh, M.; Kulinich, S.A. Anti-Icing Performance of Superhydrophobic Surfaces. *Appl Surf Sci* **2011**, *257*, 6264–6269, doi:10.1016/j.apsusc.2011.02.057.

9. Arianpour, F.; Farzaneh, M.; Kulinich, S.A. Hydrophobic and Ice-Retarding Properties of Doped Silicone Rubber Coatings. *Appl Surf Sci* **2013**, *265*, 546–552, doi:10.1016/j.apsusc.2012.11.042.

10. Wang, Y.; Yao, X.; Chen, J.; He, Z.; Liu, J.; Li, Q.; Wang, J.; Jiang, L. Organogel as Durable Anti-Icing Coatings. *Sci China Mater* **2015**, *58*, 559–565, doi:10.1007/s40843-015-0069-7.

11. Juuti, P.; Haapanen, J.; Stenroos, C.; Niemelä-Anttonen, H.; Harra, J.; Koivuluoto, H.; Teisala, H.; Lahti, J.; Tuominen, M.; Kuusipalo, J.; et al. Achieving a Slippery, Liquid-Infused Porous Surface with Anti-Icing Properties by Direct Deposition of Flame Synthesized Aerosol Nanoparticles on a Thermally Fragile Substrate. *Appl Phys Lett* **2017**, *110*, doi:10.1063/1.4981905.

12. Coady, M.J.; Wood, M.; Wallace, G.Q.; Nielsen, K.E.; Kietzig, A.M.; Lagugné-Labarthet, F.; Ragogna, P.J. Icephobic Behavior of UV-Cured Polymer Networks Incorporated into Slippery Lubricant-Infused Porous Surfaces: Improving SLIPS Durability. *ACS Appl Mater Interfaces* **2018**, *10*, 2890–2896, doi:10.1021/acsami.7b14433.

13. Liu, Q.; Yang, Y.; Huang, M.; Zhou, Y.; Liu, Y.; Liang, X. Durability of a Lubricant-Infused Electrospray Silicon Rubber Surface as an Anti-Icing Coating. *Appl Surf Sci* **2015**, *346*, 68–76, doi:10.1016/j.apsusc.2015.02.051.

14. Heydarian, S.; Jafari, R.; Momen, G. Icephobic Behavior of a Slippery Coating Containing Nanoporous Particles as Lubricant-Loaded Carriers. *Surfaces and Interfaces* **2023**, *41*, doi:10.1016/j.surfin.2023.103306.

15. Yeong, Y.H.; Milionis, A.; Loth, E.; Sokhey, J. Self-Lubricating Icephobic Elastomer Coating (SLIC) for Ultralow Ice Adhesion with Enhanced Durability. *Cold Reg Sci Technol* **2018**, *148*, 29–37, doi:10.1016/j.coldregions.2018.01.005.

16. Wang, C.; Fuller, T.; Zhang, W.; Wynne, K.J. Thickness Dependence of Ice Removal Stress for a Polydimethylsiloxane Nanocomposite: Sylgard 184. *Langmuir* **2014**, *30*, 12819–12826, doi:10.1021/la5030444.

17. Pang, H.; Zhou, S.; Gu, G.; Wu, L. Long-Term Hydrophobicity and Ice Adhesion Strength of Latex Paints Containing Silicone Oil Microcapsules. *J Adhes Sci Technol* **2013**, *27*, 46–57, doi:10.1080/01694243.2012.701503.

18. Zhuo, Y.; Wang, F.; Xiao, S.; He, J.; Zhang, Z. One-Step Fabrication of Bioinspired Lubricant-Regenerable Icephobic Slippery Liquid-Infused Porous Surfaces. *ACS Omega* **2018**, *3*, 10139–10144, doi:10.1021/acsomega.8b01148.

19. Zhu, L.; Xue, J.; Wang, Y.; Chen, Q.; Ding, J.; Wang, Q. Ice-Phobic Coatings Based on Silicon-Oil-Infused Polydimethylsiloxane. *ACS Appl Mater Interfaces* **2013**, *5*, 4053–4062, doi:10.1021/am400704z.

20. Golovin, K.; Kobaku, S.P.R.; Lee, D.H.; DiLoreto, E.T.; Mabry, J.M.; Tuteja, A. Designing Durable Icephobic Surfaces. *Sci Adv* **2016**, *2*, doi:10.1126/sciadv.1501496.

21. Wong, W.S.Y.; Hauer, L.; Naga, A.; Kaltbeitzel, A.; Baumli, P.; Berger, R.; D'Acunzi, M.; Vollmer, D.; Butt, H.J. Adaptive Wetting of Polydimethylsiloxane. *Langmuir* **2020**, *36*, 7236–7245, doi:10.1021/acs.langmuir.0c00538.

22. Butt, H.J.; Berger, R.; Steffen, W.; Vollmer, D.; Weber, S.A.L. Adaptive Wetting - Adaptation in Wetting. *Langmuir* **2018**, *34*, 11292–11304, doi:10.1021/acs.langmuir.8b01783.

23. Zhao, B.; Bonaccurso, E.; Auernhammer, G.K.; Chen, L. Elasticity-to-Capillarity Transition in Soft Substrate Deformation. *Nano Lett* **2021**, *21*, 10361–10367, doi:10.1021/acs.nanolett.1c03643.

24. Xu, Q.; Wilen, L.A.; Jensen, K.E.; Style, R.W.; Dufresne, E.R. Viscoelastic and Poroelastic Relaxations of Soft Solid Surfaces. *Phys Rev Lett* **2020**, *125*, doi:10.1103/PhysRevLett.125.238002.

25. Zhuo, Y.; Xiao, S.; Amirfazli, A.; He, J.; Zhang, Z. Polysiloxane as Icephobic Materials – The Past, Present and the Future. *Chemical Engineering Journal* 2021, *405*.

26. Liu, Y.; Ma, L.; Wang, W.; Kota, A.K.; Hu, H. An Experimental Study on Soft PDMS Materials for Aircraft Icing Mitigation. *Appl Surf Sci* **2018**, *447*, 599–609, doi:10.1016/j.apsusc.2018.04.032.

27. Glover, J.D.; McLaughlin, C.E.; McFarland, M.K.; Pham, J.T. Extracting Uncrosslinked Material from Low Modulus Sylgard 184 and the Effect on Mechanical Properties. *Journal of Polymer Science* **2020**, *58*, 343–351, doi:10.1002/pol.20190032.

28. Ibáñez-Ibáñez, P.F.; Montes Ruiz-Cabello, F.J.; Cabrerizo-Vílchez, M.A.; Rodríguez-Valverde, M.A. Ice Adhesion of PDMS Surfaces with Balanced Elastic and Water-Repellent Properties. *J Colloid Interface Sci* **2022**, *608*, 792–799, doi:10.1016/j.jcis.2021.10.005.

29. Qi, H.; Lei, X.; Gu, J.; Zhang, Y.; Gu, X.; Zhao, G.; Yu, J. Low Modulus of Polydimethylsiloxane Organogel Coatings Induced Low Ice Adhesion. *Prog Org Coat* **2023**, *177*, doi:10.1016/j.porgcoat.2023.107435.

30. Zheng, H.; Liu, G.; Nienhaus, B.B.; Buddingh, J. V. Ice-Shedding Polymer Coatings with High Hardness but Low Ice Adhesion. *ACS Appl Mater Interfaces* **2022**, *14*, 6071–6082, doi:10.1021/acsami.1c23483.

31. Meuler, A.J.; Smith, J.D.; Varanasi, K.K.; Mabry, J.M.; McKinley, G.H.; Cohen, R.E. Relationships between Water Wettability and Ice Adhesion. *ACS Appl Mater Interfaces* **2010**, *2*, 3100–3110, doi:10.1021/am1006035.

32. He, Z.; Vågenes, E.T.; Delabahan, C.; He, J.; Zhang, Z. Room Temperature Characteristics of Polymer-Based Low Ice Adhesion Surfaces. *Sci Rep* **2017**, *7*, doi:10.1038/srep42181.

33. Wang, Z.; Zhao, Z.; Wen, G.; Zhu, Y.; Chen, J.; Jing, X.; Sun, S.; Zhang, L.; Liu, X.; Chen, H. Fracture-Promoted Ultraslippery Ice Detachment Interface for Long-Lasting Anti-Icing. *ACS Nano* **2023**, *17*, 13724–13733, doi:10.1021/acsnano.3c03023.

34. Kendall, K. The Adhesion and Surface Energy of Elastic Solids. *Journal of Physics D: Applied* **1971**, *4*, 1186.

35. Beemer, D.L.; Wang, W.; Kota, A.K. Durable Gels with Ultra-Low Adhesion to Ice. *J Mater Chem A Mater* **2016**, *4*, 18253–18258, doi:10.1039/c6ta07262c.

36. Wang, Z.; Zhao, Z.; Wen, G.; Zhu, Y.; Chen, J.; Jing, X.; Sun, S.; Zhang, L.; Liu, X.; Chen, H. Fracture-Promoted Ultraslippery Ice Detachment Interface for Long-Lasting Anti-Icing. *ACS Nano* **2023**, doi:10.1021/acsnano.3c03023.

37. Müller, A.; Wapler, M.C.; Wallrabe, U. A Quick and Accurate Method to Determine the Poisson's Ratio and the Coefficient of Thermal Expansion of PDMS. *Soft Matter* **2019**, *15*, 779–784, doi:10.1039/c8sm02105h.

625 38. Johnston, I.D.; McCluskey, D.K.; Tan, C.K.L.; Tracey, M.C. Mechanical
626 Characterization of Bulk Sylgard 184 for Microfluidics and Microengineering. *Journal*
627 *of Micromechanics and Microengineering* **2014**, *24*, doi:10.1088/0960-
628 1317/24/3/035017.

629 39. Petit, J.; Bonaccurso, E. General Frost Growth Mechanism on Solid Substrates with
630 Different Stiffness. *Langmuir* **2014**, *30*, 1160–1168, doi:10.1021/la404084m.

631 40. Xue, L.; Pham, J.T.; Iturri, J.; Del Campo, A. Stick-Slip Friction of PDMS Surfaces for
632 Bioinspired Adhesives. *Langmuir* **2016**, *32*, 2428–2435,
633 doi:10.1021/acs.langmuir.6b00513.

634 41. Moučka, R.; Sedlačík, M.; Osička, J.; Pata, V. Mechanical Properties of Bulk Sylgard
635 184 and Its Extension with Silicone Oil. *Sci Rep* **2021**, *11*, doi:10.1038/s41598-021-
636 98694-2.

637 42. Chen, L.; Bonaccurso, E.; Deng, P.; Zhang, H. Droplet Impact on Soft Viscoelastic
638 Surfaces. *Phys Rev E* **2016**, *94*, doi:10.1103/PhysRevE.94.063117.

639 43. Yang, L.; Liu, X.; Wang, J.; Zhang, P. An Experimental Study on Complete Droplet
640 Rebound from Soft Surfaces: Critical Weber Numbers, Maximum Spreading, and
641 Contact Time. *Langmuir* **2023**, doi:10.1021/acs.langmuir.3c03126.

642 44. Regulagadda, K.; Gerber, J.; Schutzius, T.M.; Poulikakos, D. Microscale Investigation
643 on Interfacial Slippage and Detachment of Ice from Soft Materials. *Mater Horiz* **2022**,
644 *9*, 1222–1231, doi:10.1039/d1mh01993g.

645 45. Rønneberg, S.; Zhuo, Y.; Laforte, C.; He, J.; Zhang, Z. Interlaboratory Study of Ice
646 Adhesion Using Different Techniques. *Coatings* **2019**, *9*,
647 doi:10.3390/coatings9100678.

648 46. Rehfeld, N.; Brassard, J.D.; Yamazaki, M.; Sakaue, H.; Balordi, M.; Koivuluoto, H.;
649 Mora, J.; He, J.; Pervier, M.L.; Dolatabadi, A.; et al. Round-Robin Study for Ice
650 Adhesion Tests. *Aerospace* **2024**, *11*, doi:10.3390/aerospace11020106.

651 47. Xie, Q.; Hao, T.; Wang, C.; Kang, Z.; Shi, Z.; Zhang, J. The Mechanical Mechanism
652 and Influencing Factors of Ice Adhesion Strength on Ice-Phobic Coating. *J Mar Sci*
653 *Eng* **2021**, *9*, doi:10.3390/jmse9030315.

48. Kim, J.H.; Kim, M.J.; Lee, B.; Chun, J.M.; Patil, V.; Kim, Y.S. Durable Ice-Lubricating Surfaces Based on Polydimethylsiloxane Embedded Silicone Oil Infused Silica Aerogel. *Appl Surf Sci* **2020**, *512*, doi:10.1016/j.apsusc.2020.145728.

49. Akbari, R.; Antonini, C. Contact Angle Measurements: From Existing Methods to an Open-Source Tool. *Adv Colloid Interface Sci* 2021, *294*.

50. Stendardo, L.; Gastaldo, G.; Budinger, M.; Pommier-Budinger, V.; Tagliaro, I.; Ibáñez-Ibáñez, P.F.; Antonini, C. Reframing Ice Adhesion Mechanisms on a Solid Surface. *Appl Surf Sci* **2023**, 158462, doi:10.1016/j.apsusc.2023.158462.

51. Tagliaro, I.; Radice, V.; Nisticò, R.; Antonini, C. Chitosan Electrolyte Hydrogel with Low Ice Adhesion Properties. *Colloids Surf A Physicochem Eng Asp* **2024**, *700*, doi:10.1016/j.colsurfa.2024.134695.

52. Ibáñez-Ibáñez, P.F.; Montes Ruiz-Cabello, F.J.; Cabrerizo-Vílchez, M.A.; Rodríguez-Valverde, M.A. Contact Line Relaxation of Sessile Drops on PDMS Surfaces: A Methodological Perspective. *J Colloid Interface Sci* **2021**, *589*, 166–172, doi:10.1016/j.jcis.2020.12.093.

53. Ibáñez-Ibáñez, P.F.; Montes Ruiz-Cabello, F.J.; Cabrerizo-Vílchez, M.A.; Rodríguez-Valverde, M.A. Mechanical Durability of Low Ice Adhesion Polydimethylsiloxane Surfaces. *ACS Omega* **2022**, *7*, 20741–20749, doi:10.1021/acsomega.2c01134.

54. Krawczyk, J.; Croce, S.; McLeish, T.C.B.; Chakrabarti, B. Elasticity Dominated Surface Segregation of Small Molecules in Polymer Mixtures. *Phys Rev Lett* **2016**, *116*, doi:10.1103/PhysRevLett.116.208301.

55. Xue, L.; Pham, J.T.; Iturri, J.; Del Campo, A. Stick-Slip Friction of PDMS Surfaces for Bioinspired Adhesives. *Langmuir* **2016**, *32*, 2428–2435, doi:10.1021/acs.langmuir.6b00513.

56. Viswanathan, K.; Chandrasekar, S. Fifty Years of Schallamach Waves: From Rubber Friction to Nanoscale Fracture. *Philosophical Transactions of the Royal Society A: Mathematical, Physical and Engineering Sciences* 2022, *380*.

57. Chaudhury, M.K.; Kim, K.H. Shear-Induced Adhesive Failure of a Rigid Slab in Contact with a Thin Confined Film. *European Physical Journal E* **2007**, *23*, 175–183, doi:10.1140/epje/i2007-10171-x.

58. Viswanathan, K.; Sundaram, N.K.; Chandrasekar, S. Stick-Slip at Soft Adhesive Interfaces Mediated by Slow Frictional Waves. *Soft Matter* **2016**, *12*, 5265–5275, doi:10.1039/c6sm00244g.

59. Yamaguchi, T.; Ohmata, S.; Doi, M. Regular to Chaotic Transition of Stick-Slip Motion in Sliding Friction of an Adhesive Gel-Sheet. *Journal of Physics Condensed Matter* **2009**, *21*, doi:10.1088/0953-8984/21/20/205105.

60. Viswanathan, K.; Sundaram, N.K.; Chandrasekar, S. Stick-Slip at Soft Adhesive Interfaces Mediated by Slow Frictional Waves. *Soft Matter* **2016**, *12*, 5265–5275, doi:10.1039/c6sm00244g.

61. Golovin, K.; Tuteja, A. *A Predictive Framework for the Design and Fabrication of Icephobic Polymers*; 2017;

62. Golovin, K.; Dhyani, A.; Thouless, M.D.; Tuteja, A. *Low-Interfacial Toughness Materials for Effective Large-Scale Deicing*; 2019; Vol. 364;.

63. Mohseni, M.; Dijvejin, Z.A.; Golovin, K. Designing Scalable Elastomeric Anti-Fouling Coatings: Shear Strain Dissipation via Interfacial Cavitation. *J Colloid Interface Sci* **2021**, *589*, 556–567, doi:10.1016/j.jcis.2021.01.019.

64. Allahdini, A.; Jafari, R.; Momen, G. Transparent Non-Fluorinated Superhydrophobic Coating with Enhanced Anti-Icing Performance. *Prog Org Coat* **2022**, *165*, doi:10.1016/j.porgcoat.2022.106758.

65. Farahani, E.; Liberati, A.C.; Moreau, C.; Dolatabadi, A.; Stoyanov, P. Comparative Evaluation of the Shear Adhesion Strength of Ice on PTFE Solid Lubricant. *Lubricants* **2023**, *11*, doi:10.3390/lubricants11030105.

66. Maghsoudi, K.; Vazirinasab, E.; Momen, G.; Jafari, R. Icephobicity and Durability Assessment of Superhydrophobic Surfaces: The Role of Surface Roughness and the Ice Adhesion Measurement Technique. *J Mater Process Technol* **2021**, *288*, doi:10.1016/j.jmatprotec.2020.116883.

67. Gresham, I.J.; Lilley, S.G.; Nelson, A.R.J.; Koynov, K.; Neto, C. Nanostructure Explains the Behavior of Slippery Covalently Attached Liquid Surfaces. *Angewandte Chemie - International Edition* **2023**, *62*, doi:10.1002/anie.202308008.

68. Gresham, I.J.; Neto, C. Advances and Challenges in Slippery Covalently-Attached Liquid Surfaces. *Adv Colloid Interface Sci* 2023, *315*.

69. Walker, D.A.; Hedrick, J.L.; Mirkin, C.A. *Rapid, Large-Volume, Thermally Controlled 3D Printing Using a Mobile Liquid Interface*; 2018;

70. Wu, L.; Dong, Z.; Du, H.; Li, C.; Fang, N.X.; Song, Y. Bioinspired Ultra-Low Adhesive Energy Interface for Continuous 3D Printing: Reducing Curing Induced Adhesion. *Research* **2018**, *2018*, doi:10.1155/2018/4795604.

71. Chaudhary, R.; Akbari, R.; Antonini, C. Rational Design and Characterization of Materials for Optimized Additive Manufacturing by Digital Light Processing. *Polymers (Basel)* **2023**, *15*, doi:10.3390/polym15020287.

Acknowledgements

This project has received funding from the European Union's Horizon 2020 research and innovation programme under the Marie Skłodowska-Curie grant agreement No 956703.

P.F.I.I acknowledges the funding from the Margarita Salas grant (Ministerio de Universidades, Next Generation EU)